SPECIAL TOPIC — Magnetism, magnetic materials, and interdisciplinary research

Electronic structure & yield strength prediction for dislocation–Mo complex in the γ phase of nickel-based superalloys*

Feng-Hua Liu(刘凤华)[1] and Chong-Yu Wang(王崇愚)[1,2,†]

[1] Central Iron and Steel Research Institute, Beijing 100081, China
[2] Department of Physics, Tsinghua University, Beijing 100084, China

(Received 8 May 2017; published online 8 June 2017)

Molybenum's effects when added in the γ phase of nickel-based superalloys were studied using the lattice Green's function multiscale method. The electronic structure of the dislocation–Mo complex was analyzed and hybridization was found to contribute to the strengthening. Moreover, by combining the interaction energies calculated from two scales, the yield stress was theoretically predicted at 0 K and finite temperature.

Keywords: electronic structure, dislocation–Mo complex, critical resolved shear stress

PACS: 61.72.Yx, 61.82.Bg, 71.15.Mb **DOI:** 10.1088/1674-1056/26/7/076104

1. Introduction

Nickel-based single crystal (SC) superalloys have been widely used to manufacture advanced gas turbines due to their excellent high-temperature performance.[1,2] With the increasing demand of service performance, several refractory elements have been added into SC superalloys, such as Re, W, Mo, and Ta. Take the CMSX series of SC superalloys for example — the refractory element content of the first generation alloy (CMSX-2) is about 14.6 wt.%, while in the second (CMSX-4) and the third generation (CMSX-10) alloys, it is 16.4 wt.% and 20.7 wt.%, respectively.[3] Owing to molybdenum's lower density and lower cost, Mo substitution for Re has been considered as an alloy design approach.[4,5] Recently, Rettig designed new Re-free low-density superalloys[6] with high Mo-content. Despite the fact that they contain no Re, the creep strength of the new alloys is comparable to that of CMSX-4 alloys. Therefore, the alloying effect of Mo will be necessary to understanding the mechanism of Mo-strengthening of SC superalloys.

Molybdenum tends to partition to the γ matrix,[7,8] and scanning electron microscope (SEM) experiments have shown that most dislocations are in the γ channel.[9,10] Dislocation is one of the important defects in SC alloys and its geometrical feature and motion behavior greatly affect the mechanical properties of these materials. In this regard, dislocation–Mo interaction is important. In recent years, with the development of multiscale methods, simulation of dislocation-doping has become more and more feasible and accessible.[11,12] However, research on the effects of dislocation–Mo interaction on electronic structure and mechanical properties of Ni-based SC superalloys has been very limited. Using the lattice Green's function (LGF) multiscale method, equilibrium dislocation cores in Ti and Al have been modeled by quantum mechanical approaches.[13,14] Therefore, we adopted the LGF multiscale method to simulate the dislocation core in theγ matrix. The primary purpose of this work is to investigate the alloying effects of Mo in a dislocation system by employing a multiscale method. Besides analyzing the electronic structure from first principles, we also predicted the increase in macroscopic yield stress brought about by Mo addition by combining first-principles calculations with continuum elasticity theory.

2. Electronic structure analysis of dislocation–Mo interaction

In this section, we report our first-principles calculations of the dislocation–Mo complex to get the interaction energy between the two crystal defects and the electronic structure of the complex.

2.1. Model & methods for electronic structure calculations

In this section, we employed the equilibrium dislocation core in the γ Ni matrix that we obtained by the LGF multiscale method.[15] The simulation model of the edge dislocation was in a 50 Å×50 Å×4.311 Å cell along the $x\,[\bar{1}10]$, $y\,[111]$, and $z\,[11\bar{2}]$ directions, containing 495 atoms. The vacuum boundary conditions were applied in the x and y directions, while in the z direction the dislocation line direction periodic condition was introduced. A fragment of the central part of the dislocation core is shown in Fig. 1, in which the atoms are colored according to their local coordination structure. The stacking fault between two partial dislocations has an HCP structure, and it is denoted by magenta atoms. The gray atoms represent

*Project supported by Beijing Municipality Science & Technology Commission, China (Grant No. D161100002416001).
†Corresponding author. E-mail: cywang@mail.tsinghua.edu.cn
© 2017 Chinese Physical Society and IOP Publishing Ltd

the two Shockley partial dislocations and the blue atoms represent atoms with FCC structure. The equilibrium dislocation core structure is the essential basis for the electronic structure calculations.

First-principles calculations were performed to get the interaction energy between the Mo atom and the dislocation core, as well as the electronic structure. The substitution sites for the interaction energy calculation are labeled as 1–22 in Fig. 1. We used density functional theory (DFT), implemented using the Vienna *ab-initio* simulation package (VASP),[16,17] the projector augmented wave method,[18,19] and the generalized gradient approximation in the parameterization introduced by Perdew, Burke and Ernzerhof.[20] Plane waves have been included up to a cutoff energy of 300 eV. The Fermi surface was smeared out using the Methfessel–Paxton smearing scheme[21] taking $\sigma = 0.2$ eV.

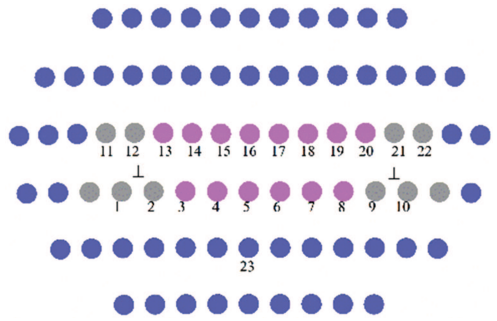


Fig. 1. (color online) Fragment of the central dislocation core labeled with substitution sites (1–22) for solute atoms for interaction energy calculations.

2.2. Dislocation–Mo interaction energy in dislocation core region

The interaction energy at site (x_i, y_j) is defined as the difference between the energy of the cell with the Mo atom in the dislocation core and the reference energy when the Mo atom is located at infinity

$$E_{\text{inter}}(x_i, y_j) = E_{\text{dis-Mo}}(x_i, y_j) - E_{\text{ref}}. \quad (1)$$

Mo atoms substitute for Ni atoms in the positions labeled 1–22 in Fig. 1, in both the compressed and the dilated regions of the dislocation.

The dislocation–Mo interaction energies computed by DFT on both sides are shown in Fig. 2. In accordance with the continuum medium theory, the interaction energies are negative in the dilated region, which indicates a higher occupation probability and segregation for Mo solute atoms and a strong binding between Mo atoms and dislocations when dislocations glide; therefore adding Mo can promote the strength of the alloy. While on the compressed side, the interactions are positive, meaning that the substitution positions in this region are energetically less favorable. Besides, a simple symmetry can be seen in the interaction energy values — the same symmetry found in the dislocation structure. From Fig. 2, we see that most binding positions lie in the immediate dislocation core, which corresponds to the stacking fault region as shown in Fig. 1. As a result, high probability of Suzuki segregation will be guaranteed and will finally lead to increased strength of the alloy.

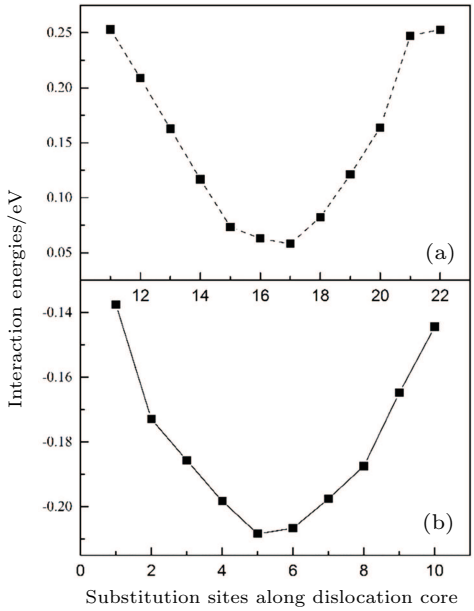


Fig. 2. (color online) Position-dependent dislocation–Mo interaction energies in both (a) the compressed and (b) the dilated regions of the dislocation.

2.3. Electronic structure analysis

It is widely recognized that the electronic effect of impurity atoms plays a significant role in the mechanical properties of the alloys. When foreign atoms enter the alloys, the electronic structure of the system and the bonding characteristics are seriously affected. Below further exploration of the physical origin of the interaction between foreign atoms and the dislocations yields the local density of states (LDOS) and the charge density difference (CDD).

The most stable structure for the dislocation–Mo complex system is the configuration wherein Mo substitutes in a Ni5 site as shown in Fig. 2. Based on the most stable configuration, the LDOS and CDD were calculated.

In Fig. 3, the LDOS of Mo and its nearest-neighbor (NN) (from FNN to 3rd NN) atoms are plotted in solid lines, along with the LDOS of the corresponding NN Ni atoms in a pure dislocation system for comparison (dashed lines). Obviously, changes of LDOS take place mainly on the FNN and 2nd NN atoms. The LDOS of the FNN and 2nd NN atoms decrease greatly at the Fermi level E_F and peaks at E_F shift downward to energy values that are lower than those of the corresponding atoms in pure dislocation. This implies that the electrons on the Fermi surface transfer to a deeper valence band, resulting in less chemical activity and a low excitation transition probability increasing the stability of the Modoped alloy. At the

lower edge and in the middle of the valence band, any formation of hybrid peaks is notable. In particular, the hybrid peaks of the FNN atoms are more intense than those of the 2nd NN atoms. However, the LDOS of the 3rd NN Ni atoms hardly change over the whole energy region, indicating that a solute Mo atom has little effect on its 3rd NN atoms; therefore the effect of Mo is quite localized in the matrix. To further investigate the chemical interaction between dislocation and solute Mo, the partial density of states (PDOS) of NN Ni atoms and Mo should be analyzed. As the Ni6 atom is on the slip plane, we took Ni6 as a typical atom to analyze the PDOS.

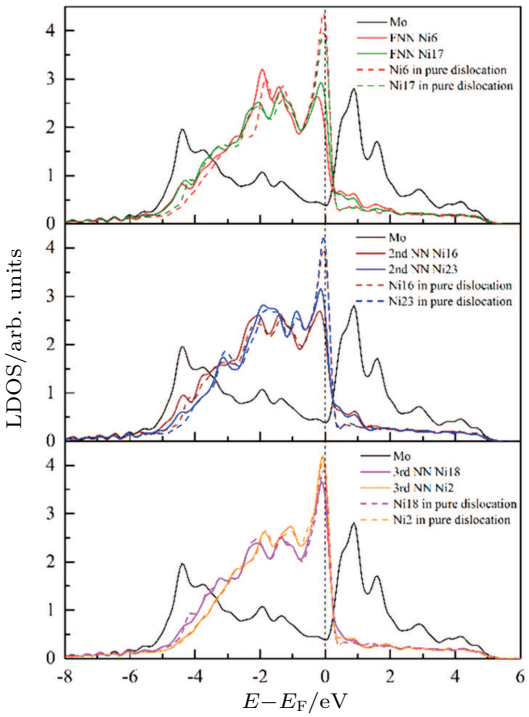


Fig. 3. (color online) LDOS of Mo and its nearest-neighbor atoms in a doped dislocation core (solid lines) and the corresponding atoms in a pure dislocation core (dashed lines).

The PDOSs of Mo and its FNN Ni6 atoms are shown in Fig. 4; to represent the influence of Mo solute on a Ni6 atom, the PDOS of a Ni6 atom in a pure dislocation core is plotted as well in dashed curves. With the introduction of Mo solute, the s-states and p-states of a Ni6 atom are hardly affected, whereas its d-states are strongly influenced, especially at the Fermi level and at the lower edge of the valence band. Hybridization between Ni6 and Mo is mainly d-d hybridization. At around −4.4 eV, hybrid peaks are found on Ni6 3d states in Modoped dislocation, but not found for the corresponding atom in pure dislocation. In the middle of the valence band, hybrid peaks are also found in Mo-doped dislocation. More detailed analysis of the fivefold d-orbital indicates that the bonding states around −4.4 eV can be further assigned to the ddδ (Mo 4d t_{2g}–Ni 3d t_{2g}) and ddπ (Mo 4d e_gNi 3d e_g) hybrid states, while at around −1.4 eV ddπ (Mo 4d e_g–Ni 3d e_g) hybrid states can also be found to form antibonding states. However, nonbonding states exist between Ni6 and Mo atoms near the Fermi level. Moreover, with Mo added, there is an increase of 0.13 and 0.11 states occupying Ni6 d–t_{2g} and Ni6 d–e_g, respectively. This suggests that charge would transfer into Ni t_{2g} and e_g orbitals — a redistribution of electrons — which would be revealed by the CDD.

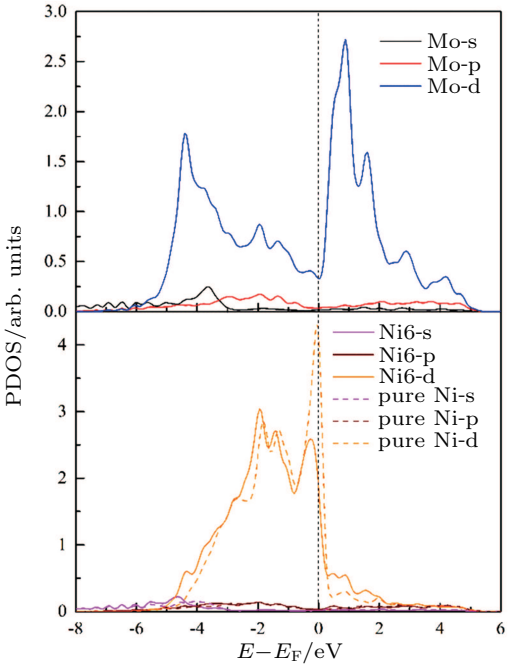


Fig. 4. (color online) PDOS of Mo and its FNN Ni6 atoms shown in solid lines; dashed lines denote the PDOS of Ni6 in pure dislocation.

The CDD maps describing charge accumulation and depletion can characterize the bond strength and charge transfer. Figure 5 shows a CDD contour plot of the (111) slip plane of dislocation doped with Mo atoms. The red areas correspond to an increase of electron density, while the density of blue areas is diminished. One can see that directional bonds are formed between Ni–Mo pairs, which can be seen as a manifestation of electron redistribution around the Mo atom.

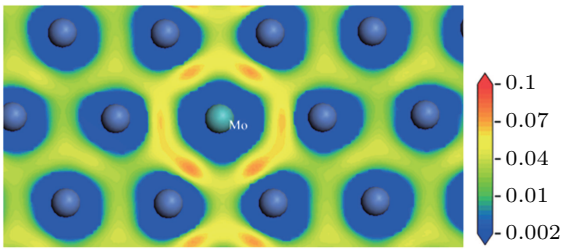


Fig. 5. (color online) Charge density difference with respect to Modoped dislocation core in the (111) plane. The color scale of CDD is in units of e/(a.u.)^3.

Overall, from the analysis of DOS and CDD, we can conclude that the addition of Mo to a Ni matrix benefits formation of hybrid peaks, which can promote the bond strength between dislocations and solute Mo atoms.

3. Prediction of resolved shear stress of Mo-doped Ni matrix by first-principles calculation

3.1. Theoretical background

As we discussed in Section 2, Mo can affect microscopic bonding states and distribution of electrons. Thus, it can influence macroscopic mechanical properties. It is widely known that Mo and other refractory elements such as Re and W have been doped in Ni-based superalloys to increase the yield strength through solid-solution strengthening.[22,23] The yield strength is a critical parameter in mechanical performance. Therefore, predictability of the increase of yield strength caused by adding Mo would be helpful for alloy design.

Solute strengthening is closely related to the increase of flow stress of a metal owing to the presence of solute atoms.[24] One of the fundamental physical origins of solute strengthening is the interaction between the strain field of the dislocations and solute atoms when these atoms are introduced into lattice sites in and around the dislocation core.[25] Two classical models introduced in 1948[24] describe the hardening mechanism — the Friedel–Fleischer model and the Labusch model. The Friedel–Fleischer model applies to a dilute solid solution and regards the solute atoms as discrete obstacles,[26] so it can also be classified as strong pinning. In contrast, the weak pinning proposed by Labusch considers the collective interaction of many solute atoms around a dislocation and attributes strengthening to the occurrence of favorable statistical fluctuation in the solute configuration.[27,28] It is well known that the effect of quantitative mechanics (QM) should be considered in solid solution strengthening, especially when the solutes are located in the very core and along the stacking fault of the dislocation. Our analysis of electronic structure in Section 2 also shows that interactions between solute atoms in the immediate core and dislocations should be emphasized; however, they are ignored in continuum medium elasticity theory.

For the present work, we adopted the method proposed by Leyson[29] to calculate the critical resolved shear stress (CRSS) of a Ni matrix doped with solute Mo atoms. The method considers interaction energy across multiple length scales by combining first-principles calculations

$$E_{\text{inter}}(x_i, y_j) = E_{\text{dis-doping}}(x_i, y_j) - E_{\text{ref}} \tag{2}$$

with elasticity calculations

$$U_{\text{elastic}} = -p\Delta V, \tag{3}$$

where p is the stress field of the dislocation in classical elasticity theory, and ΔV is the misfit volume which can be obtained from first-principles calculations.

It is based on the following general physical picture: a straight dislocation of length L bows out in the glide plane seeking favorable local environments of random solute atoms to minimize potential energy. The typical configuration of the dislocation is determined by two competing processes — increasing the binding energy and decreasing the elastic energy. These two processes result in two characteristic length parameters, including the bowing segment length ξ_c and the bow-out distance w_c. These characteristic lengths can be determined by minimizing the total energy change$\Delta E_{\text{tot}}(\xi, w)$, such that

$$\Delta E_{\text{tot}}(\xi, w) = \left[\left(\Gamma\frac{w^2}{2\xi}\right) + \Delta E_{\text{p}}(\xi, w)\right]\left(\frac{L_0}{2\xi}\right), \tag{4}$$

where Γ is the line tension of the dislocation, which can be derived from the formula[30]

$$\Gamma = \frac{\mu b^2}{8\pi(1-\upsilon)}(2 - \upsilon + 3\upsilon\cos 2\theta). \tag{5}$$

Here, b is the Burgers vector, θ is the angle between b and the dislocation line, μ is the shear modulus, and υ is Poisson's ratio. Minimizing the total energy change $\Delta E_{\text{tot}}(\xi, w)$, the energy barrier preventing the dislocation to glide is obtained as follows:

$$\Delta E_{\text{b}} = \left(\frac{4\sqrt{2}-1}{3}\cdot\frac{3^{5/6}}{2^{5/3}}\right)\left(\frac{cw_{\text{c}}^2\Gamma\Delta\tilde{E}_{\text{p}}^2(w_{\text{c}})}{b}\right)^{1/3}. \tag{6}$$

The strength of a material depends on how easily dislocations propagate in its crystal lattice. Therefore, the zero-temperature yield strength τ_{y0} corresponds to the stress at which the dislocation escapes from the energy barrier, and it can be predicted as

$$\tau_{\text{y0}} = 1.01\left(\frac{c^2\Delta\tilde{E}_{\text{p}}^4(w_{\text{c}})}{\Gamma b^5 w_{\text{c}}^5}\right)^{1/3}. \tag{7}$$

For a quasi static loading, the stress at low temperature follows

$$\tau_{\text{y}}(T) = \tau_{\text{y0}}\left[1 - \left(\frac{kT}{\Delta E_{\text{b}}}\ln\frac{\dot{\varepsilon}_0}{\dot{\varepsilon}}\right)^{2/3}\right]. \tag{8}$$

It is obvious that at elevated temperatures, movement of a dislocation could be thermally activated at stresses below τ_{y0}. A detailed calculation can be found in Ref. [26].

3.2. First-principles calculations of the parameters for elasticity computation

In this section, the elastic parameters and misfit volume, which are essential input to continuum elasticity theory calculations were obtained from DFT computations. The elastic parameters that must be calculated are the bulk modulus, the shear modulus and Poisson's ratio. We took $2\times2\times2$ supercells with a Mo atom substituted for one bulk Ni atom. The DFT computations were implemented using VASP.[16,17] PBE was selected as the exchange–correlation functional.[20] A $11\times11\times11$ Monkhorst–Pack k-mesh.[31] and a kinetic energy cutoff of 500 eV were used. The bulk modulus B was

obtained by fitting the Murnaghan equation of state,[32] and the elastic constants were obtained using the energy-strain approach.[33] Based on the equations of linear elasticity for isotropic materials,[34] the shear modulus μ and Poisson's ratio ν can be expressed as

$$\mu = \frac{3c_{44} + c_{11} - c_{12}}{5}, \tag{9}$$

$$\upsilon = \frac{3B - 2\mu}{2(3B + \mu)}. \tag{10}$$

The calculated bulk modulus B, shear modulus μ, and Poisson's ratio ν for $Ni_{31}Mo$ are $B = 197.3$ GPa, $\mu = 96.8$ GPa, and $\nu = 0.29$.

The misfit volume ΔV introduced into the Ni matrix by the Mo atom is another parameter obtained from DFT calculations. We computed the misfit volume by the formula[35,36]

$$\frac{\Delta V}{V_0} = -\left(\frac{1}{B}\frac{\partial p}{\partial c}\right) c_{1\mathrm{sol}}, \tag{11}$$

where $c_{1\mathrm{sol}}$ is the Mo concentration with only one Mo atom in the cell. Separate geometric optimizations were made in the fixed-volume supercells with one, two, and three Mo atoms. We employed two different supercells sizes containing 27 and 64 atoms, respectively, and calculated the misfit volume $\Delta V = 4.53$ Å^3.

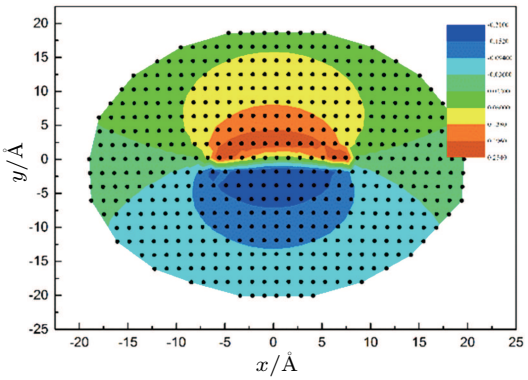


Fig. 6. (color online) Dislocation–Mo interaction energy as a function of the solute position (x_i, y_j). In the immediate dislocation core, the energy values are from first principles, and at other sites, the values are calculated from classical elasticity theory.

With the calculated misfit volume ΔV, the Mo-dislocation interaction energy can be obtained from the classical elasticity theory.

Figure 6 displays the interaction energy across multiple length scales with formulas (2) and (3). Consistency between the interaction energies computed by first principles and elasticity can be seen in Fig. 6.

3.3. Critical resolved shear stress at 0 K and finite temperature

In general, the yield stress of the γ phase is a combination of lattice frictional stress and the additional strength contributed by doping atoms. Lattice frictional stress is intrinsic resistance to dislocation movement, which can be neglected because of its small value of 0.77 MPa in any FCC crystal.[37] Hence, the yield stress of the γ-FCC phase can be taken to be the stress increase that is due to the doping atoms.

By using the elastic parameters and misfit volume from DFT calculations, together with the interaction energies from two length scales as input to the strengthening model, the critical resolved shear stress of Ni–Mo can be predicted. According to formulas (7) and (8), the zero temperature yield stress is proportional to the solute concentration to the power of 2/3, while the finite temperature stress will be affected by more factors such as concentration, strain rate and temperature. In view of the content of Mo in real superalloys, the data will be considered up to a maximum concentration of 2 at.%. CRSS dependence on Mo concentration is shown in Fig. 7 at $T = 0$ K and at $T = 78$ K. At $T = 78$ K, the strain rate takes the value of $\dot{\varepsilon} = 6.67 \times 10^{-5}$ s^{-1}. We can see that with increasing temperature, thermal activation can assist the movement of dislocations, and the CRSS $\tau_y(T)$ decreases from τ_{y0}.

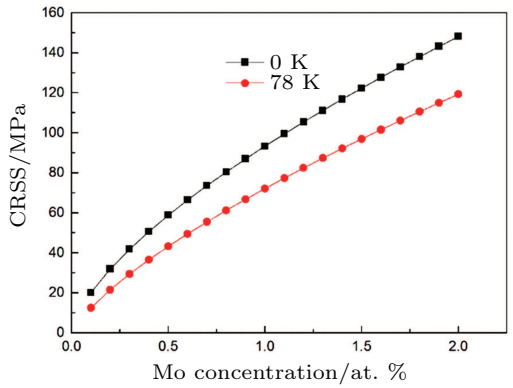


Fig. 7. (color online) CRSS as a function of the atomic fraction at temperatures $T = 0$ K and $T = 78$ K.

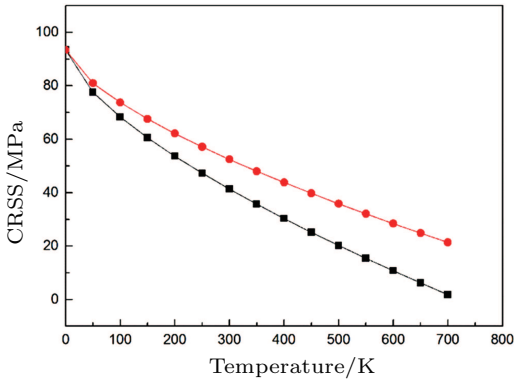


Fig. 8. (color online) Temperature dependence of CRSS under the strain rates of 6.67×10^{-5} s^{-1} (black line) and 2×10^{-2} s^{-1} (red line), respectively.

Figure 8 shows the temperature and strain rate dependence of the CRSS when the solute concentration is 1 at.%. It is clear that the predicted CRSS increases with the strain rate and decreases with the temperature. At high strain rates, more dislocation sources will be activated, which suppresses

dislocation glide in a single crystal. Therefore, a high strain rate can promote the strength of a material. Moreover, note that under high strain rate, the rate of decrease of $\tau_y(T)$ with increasing temperature turns out to be slow.

Comparison between the prediction and experiment reveals a better match for the γ phase containing a dislocation–Mo complex. The experimental flow stress value of Ni–Mo binary alloy was measured by Mishima *et al.* at $T = 78$ K and $\dot{\varepsilon} = 1.2 \times 10^{-4}$ s^{-1}.[38] The flow stress σ, which was measured using a 0.2% strain offset, is about 170 MPa when the Mo concentration is 2 at.%. Based on the Schmid law, there is a relation between σ and τ : $\sigma = m\tau$. Hence, σ can be converted into τ by multiplying $m = 0.5$. We compared our predictive results with the experiment[38] and found that our calculated CRSS is consistent with the experimental data.

4. Conclusion

Based on the lattice Green's function and firstprinciples DFT calculations, we calculated the electronic structure of dislocation–Mo complex to explore the electronic effect of Mo strengthening in the γ phase of Ni-based superalloys. The analysis indicates that adding Mo to γ phase containing dislocations benefits formation of hybrid peaks, which can promote the bond strength between dislocations and doping Mo atoms. In addition, by combining the dislocation–Mo interaction energies calculated from first principles and elasticity theory, we theoretically predicted the increased yield stress due to adding Mo at 0 K and low temperature. Our prediction for Mo doped γ phase is in good agreement with experimental values.

Acknowledgment

The authors wish to thank Dr. Lu Bao-Kun (Tsinghua University) for helpful discussions.

References

[1] Reed R C 2006 *The Superalloys: Fundamentals and Applications* (New York: Cambridge University Press)
[2] Tin S and Pollock T M 2003 *Mater. Sci. Eng. A* **348** 111
[3] Fuchs G E 2001 *Mater. Sci. Eng. A* **300** 52
[4] Mackay R A, Gabb T P, Smialek J L and Nathal M V 2010 *JOM* **62** 48
[5] Ru Y, Li S, Pei Y, Zhou J, Gong S and Xu H 2015 *J. Alloys Compd.* **662** 431
[6] Rettig R, Matuszewski K, Müller A, Helmer H E, Ritter N C and Singer R F 2016 *Development of a Low-density Rhenium-free Single Crystal Nickel-based Superalloy by Application of Numerical Multi-criteria Optimization Using Thermodynamic Calculations. International Symposium on Superalloys, Seven Springs, Pennsylvania, USA*
[7] Bagot P A J, Silk O B W, Douglas J O, Pedrazzini S, Crudden D J, Martin T L, Hardy M C, Moody M P and Reed R C 2017 *Acta Mater.* **125** 156
[8] Peng Z, Povstugar I, Matuszewski K, Rettig R, Singer R, Kostka A, Choi P P and Raabe D 2015 *Scr. Mater.* **101** 44
[9] Huang M, Cheng Z, Xiong J, Li J, Hu J, Liu Z and Zhu J 2014 *Acta Mater.* **76** 294
[10] Zhang J X, Harada H, Ro Y, Koizumi Y and Kobayashi T 2008 *Acta Mater.* **56** 2975
[11] Yu X X and Wang C Y 2009 *Acta Mater.* **57** 5914
[12] Zhang X, Wang C Y and Lu G 2008 *Phys. Rev. B* **78**
[13] Ghazisaeidi M and Trinkle D R 2012 *Acta Mater.* **60** 1287
[14] Woodward C, Trinkle D R, Jr H L and Olmsted D L 2008 *Phys. Rev. Lett.* **100**
[15] Liu F H and Wang C Y 2017 *Rsc Adv.* **7** 19124
[16] Kresse G and Furthmüller J 1996 *Phys. Rev. B* **54** 11169
[17] Kresse G and Hafner J 1993 *Phys. Rev. B* **47** 558
[18] Blöchl P E 1994 *Phys. Rev. B* **50** 17953
[19] Kresse G and Joubert D 1999 *Phys. Rev. B* **59** 1758
[20] Perdew J P, Burke K and Ernzerhof M 1996 *Phys. Rev. Lett.* **77** 3865
[21] Methfessel M and Paxton A T 1989 *Phys. Rev. B* **40** 3616
[22] Fleischmann E, Miller M K, Affeldt E and Glatzel U 2015 *Acta Mater.* **87** 350
[23] Heckl A, Neumeier S, Göken M and Singer R F 2011 *Mater. Sci. Eng. A* **528** 3435
[24] Butt M Z and Feltham P 1993 *Journal of Materials Science* **28** 2557
[25] Argon A S 2008 *Strengthening Mechanisms in Crystal Plasticity* (New York: Oxford University Press)
[26] Fleisgher R L 1961 *Acta Metall* **9** 996
[27] Labusch R 1972 *Acta Metall* **20** 917
[28] Labusch R 2006 *Phys. Status Solidi* **41** 659
[29] Leyson G P, Curtin W A, Jr H L and Woodward C F 2010 *Nat. Mater.* **9** 750
[30] Barnett D M, Asaro R J, Gavazza S D, Bacon D J and Scattergood R O 2001 *J. Phys. F: Metal Phys.* **2** 854
[31] Monkhorst H J and Pack J D 1976 *Phys. Rev. B* **13** 5188
[32] Birch F 1947 *Phys. Rev.* **71** 809
[33] Söderlind P, Eriksson O, Wills J M and Boring A M 1993 *Phys. Rev. B* **48** 5844
[34] Kim D E, Shang S L and Liu Z K 2009 *Comput. Mater. Sci.* **47** 254
[35] Giessen E V D and Needleman A 1995 *Modelling & Simulation in Materials Science & Engineering* **3** 689
[36] Vannarat S, Sluiter M H F and Kawazoe Y 2001 *Phys. Rev. B* **64** 224203
[37] Wu Z, Bei H, Pharr G M and George E P 2014 *Acta Mater.* **81** 428
[38] Mishima Y, Ochiai S, Hamao N, Yodogawa M and Suzuki T 1986 *Transactions of the Japan Institute of Metals* **27** 656